J. Fluid Mech. (1997), *vol.* 339, *pp.* 309–330. Printed in the United Kingdom

Wave diffraction by a long array of cylinders

By H. D. MANIAR AND J. N. NEWMAN

Department of Ocean Engineering, MIT, Cambridge, MA 02139, USA

(Received 19 September 1996 and in revised form 20 December 1996)

Water wave diffraction by an array of bottom-mounted circular cylinders is analysed under the assumptions of linear theory. The cylinders are identical, and equally spaced along the array. When the number of cylinders is large, but finite, near-resonant modes occur between adjacent cylinders at critical wavenumbers, and cause unusually large loads on each element of the array. These modes are associated with the existence of homogeneous solutions for the diffraction by an array which extends to infinity in both directions. This phenomenon is related to the existence of trapped waves in a channel. A second trapped wave is established, corresponding to Dirichlet boundary conditions on the channel walls, as well as a sequence of higher wavenumbers where 'nearly trapped' modes exist.

1. Introduction

Many offshore structures are supported by vertical columns of circular form, which are subject to wave diffraction and associated pressure forces or 'loads'. Linearized potential theory is applicable, provided the wave height is small in relation to the wavelength and the diameter of the columns. Plane progressive incident waves can be assumed, with wavenumber K and wavelength $\lambda = 2\pi/K$.

Special attention has been given to structures which consist of a large number of separate elements, situated in a periodic array. Applications of such structures include bridges and proposed designs for floating airports. Arrays of wave-power devices also have been proposed to take advantage of the favourable interference characteristics which exist in certain cases. Interference has an important effect on the loads, not only for large arrays but also for structures with only a few elements such as the columns of tension-leg platforms.

Various analytical methods have been developed to solve the wave diffraction problem for these types of configurations. Havelock (1940) derived the velocity potential for a single cylinder, and this solution was extended to multiple cylinders by Ohkusu (1974). More general arrays of axisymmetric bodies have been analysed by Kagemoto & Yue (1986) and Linton & Evans (1990), and in other references cited therein.

The present paper is motivated by the singular role of quasi-resonant wave interactions which we have found at critical values of the spacing of the array elements, relative to the wavelength. At these critical values we have computed very large amplitudes of the free-surface elevation between adjacent elements, and corresponding large loads acting on each cylinder. The principal objectives of this work are to emphasize and explain the occurrence of these interactions.

We consider an array of N equally spaced fixed cylinders, each having a radius a about its vertical axis. The axes of adjacent cylinders are separated by a distance

$2d$, and situated in the plane $y = 0$ of a Cartesian coordinate system (x, y, z) where $-h < z < 0$ is the fluid domain, $z = 0$ is the plane of the undisturbed free surface, and the depth h is constant.

Incident plane waves propagate in the direction with angle β relative to the $+x$-axis. The corresponding velocity potential is

$$\Phi_I(x, y, z, t) = \mathrm{Re}\left\{\phi_I(x, y)\, \mathrm{e}^{-\mathrm{i}\omega t} \cosh K(z + h)/\cosh Kh\right\}, \tag{1.1}$$

where

$$\phi_I = \mathrm{e}^{\mathrm{i}K(x\cos\beta + y\sin\beta)},$$

and a constant factor proportional to the amplitude is ignored. The frequency ω and wavenumber K are related by the dispersion relation $\omega = (gK \tanh Kh)^{1/2}$, where g is the gravitational acceleration.

The total diffraction potential $\Phi_D = \Phi_I + \Phi_S$ is defined as the sum of the incident and scattered components. Since the cylinders extend vertically throughout the fluid domain, the z-dependence of Φ_D and Φ_S is identical to that of the incident plane wave, and the diffraction potential can be written in the form

$$\Phi_D = \mathrm{Re}\left\{\phi_D(x, y)\, \mathrm{e}^{-\mathrm{i}\omega t} \cosh K(z + h)/\cosh Kh\right\}. \tag{1.2}$$

The function ϕ_D is governed by the modified wave equation

$$\nabla^2\phi_D + K^2\phi_D = 0, \tag{1.3}$$

subject to the boundary condition of zero radial velocity on each cylinder. The scattering component $\phi_S = \phi_D - \phi_I$ satisfies the radiation condition of outgoing waves in the far field.

The function $\phi_D(x, y)$ depends only on the horizontal coordinates, and can be associated physically with the diffraction of two-dimensional acoustic waves by an array of circles. In addition to the coordinates (x, y), ϕ_D depends on the normalized wavenumber Ka, the incidence angle β, and the geometrical ratio $a/d < 1$. The most significant parameter with respect to wave interference is Kd, which relates the spacing between adjacent cylinders to the wavelength.

As an example to motivate the present work, figure 1 shows the magnitude of the wave load on the middle element of an array consisting of nine cylinders, in head waves ($\beta = 0$). Two geometrical configurations are shown, where $a/d = 1/4$ and $a/d = 1/2$. Also shown for comparison is the load on a single isolated cylinder of the same radius. The most distinctive feature is a sequence of narrow peaks which occur when Kd is slightly less than $\pi/2$ times an integer. The highest peaks are about three times the force on a single cylinder; it will be shown in subsequent examples that this multiplicative factor increases without limit as $N \to \infty$. (It should be emphasized that we are considering the load on a single cylinder, not the total force on the array which would be expected to increase with N in general.)

In long wavelengths ($Ka \ll 1$), where the scattering from each cylinder is relatively weak, the load on each element is practically the same as for a single isolated cylinder. For the two cases shown in figure 1, this applies in the regime $Kd/\pi < 0.3$. For substantially larger wavenumbers, corresponding to shorter wavelengths, one might expect a reduced load on each cylinder due to sheltering except near the head of the array. This appears to be the case to some extent, except near the peaks, and the first peak seems to divide the two regimes where interactions are weak or sheltering is significant. The principal question that remains is to explain the peaks themselves.

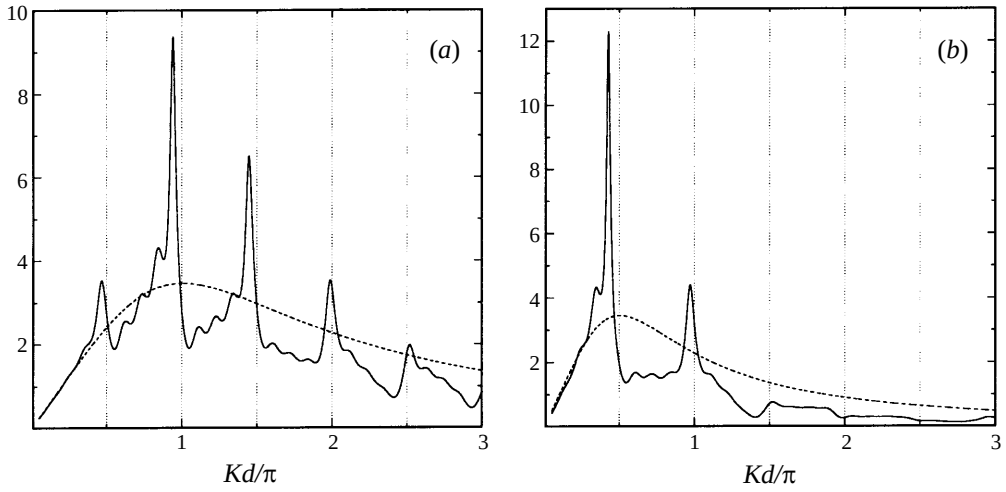

FIGURE 1. Magnitude of the load on the middle cylinder of an array $N = 9$ (solid line) and comparison with the load on a single isolated cylinder (dashed line). The propagation of the incident waves is in the direction parallel to the array ($\beta = 0$). (*a*) $a/d = 1/4$ and (*b*) $a/d = 1/2$, where a is the cylinder radius and $2d$ the spacing between adjacent cylinder axes. The magnitudes shown are normalized on the basis of unit wave amplitude, density, gravity, cylinder radius and depth.

Analogous results have been presented by Simon (1982), for the damping coefficients of an array of axisymmetric wave-energy devices, including the specific case $N = 9$ and $a/d = 1/2$. In his discussion Simon notes that the results 'become increasingly intricate, with a lot of fine structure, as the number of devices increases, and this does not add to one's understanding.' Ohkusu (1982) considers the coefficients of wave reflection and transmission by one or two cylinders in a channel, and finds sharply peaked results from both theory and experiments. Ohkusu's results are discussed in the Conclusions.

We will show that a close relation exists between the peaks in figure 1 and the trapped waves which can occur in a channel with rigid sidewalls. The existence of such trapped waves has been established by Linton & Evans (1992), Evans, Levitin & Vassiliev (1994), and in other papers referenced therein. Trapped waves have been shown to exist for circular cylinders (and other body shapes), at one critical wavenumber just below the cut-off value $Kd = \pi/2$ for antisymmetric wave propagation in the channel. The trapped wave itself is antisymmetric about the channel midplane, and hence cannot radiate energy to infinity along the channel. Since there are no antisymmetric far-field waves, and the normal velocity is zero on both the channel walls and cylinder, this mode is a homogeneous solution of the boundary-value problem. We shall refer to this subsequently as the 'Neumann trapped wave', in view of the corresponding boundary condition on the walls.

The connection with trapped waves may seem surprising since we are concerned here with diffraction of head waves past a finite array in an otherwise unbounded horizontal domain. The diffraction of beam waves ($\beta = 90°$) past an infinite array is equivalent to that of a single cylinder in a channel, in accordance with the method of images, but for other angles of wave incidence this equivalence is lost and the role of the trapped waves is less obvious. Moreover the analogy with trapped waves in a channel only explains the first peak in figure 1.

We initially found the peaks illustrated in figure 1 while analysing much larger arrays with a high-order panel program based on B-splines. The original objective was to test the accuracy and limits of this program in comparison to the interaction theory of Linton & Evans (1990). Those results, which are described in §2, provide empirical evidence of the connection with trapped waves. In subsequent sections a matrix analysis based on the theory of Linton & Evans (1990) is used to show that the trapped modes are eigensolutions not only for the diffraction problem in a channel, and for the equivalent problem of an infinite array in beam waves, but more generally for waves of arbitrary incidence angle. Moreover the second peak corresponds to a trapped wave in a non-physical channel where the velocity potential (rather than its normal derivative) vanishes on the walls. The existence of this 'Dirichlet trapped wave' is hitherto unknown to our knowledge, in the context of water waves, but analogous modes are known to exist in the acoustics context. (This analogy is discussed in §6.) The subsequent peaks in figure 1 are associated with 'nearly-trapped waves', where the radiation is weak but non-zero.

After presenting computational results for long arrays in §2, the interaction theory of Linton & Evans (1990) is re-derived in §3 and simplified for long arrays in §4. In §5 we show that the corresponding linear system of equations has homogeneous solutions, for an array with an infinite number of elements, at the wavenumbers corresponding to the Neumann and Dirichlet trapped modes. At the higher wavenumbers where secondary peaks are shown in figure 1, there is no homogeneous solution but the linear system is poorly conditioned, suggesting a large but finite response with weak radiation of energy. Conclusions are summarized in §6.

2. Computations for large arrays

Figure 2 shows the magnitude and phase of the wave load acting on each element of a long array ($N = 100$) of cylinders with the ratio $a/d = 1/2$. These results are for head waves ($\beta = 0$), at five different wavenumbers which are denoted (*a–e*). In each case the magnitude, shown in the left column, is normalized by the corresponding result for a single isolated cylinder. Except in case (*d*) the normalized magnitude on the first cylinder is approximately 1, indicating that the load on the first cylinder of the array is not strongly affected by interactions with the other elements. For the remainder of the array interactions are important, and it is necessary to distinguish between three regimes.

In the first plot (*a*), where the wavelength is three times the cylinder spacing, the load increases slowly along the array, suggesting a refraction of the incident wave energy toward the array. The phase is closely correlated with the local phase of the incident wave at each cylinder.

In cases (*c*) and (*e*), where the wavelength is shorter, the load decreases along the array due to sheltering. As in the long-wavelength regime (*a*), the phase is essentially the same as the local incident-wave elevation. Thus in (*c*), where the wavelength is twice the spacing, the forces on consecutive cylinders have opposite phase and in (*e*), where the wavelength is equal to the spacing, their phase is nearly constant.

Seeking to explain the transition from (*a*) to (*c*), we first discovered the result (*b*) at $Kd = 1.390706$. Here the normalized load is much larger, reaching a maximum value of 35 near the middle of the array. The phase differs by π between adjacent cylinders, whereas the phase difference of the incident wave over the same distance is less than 2.4. This wavenumber is virtually identical to the value $Kd = 1.39131$ reported by

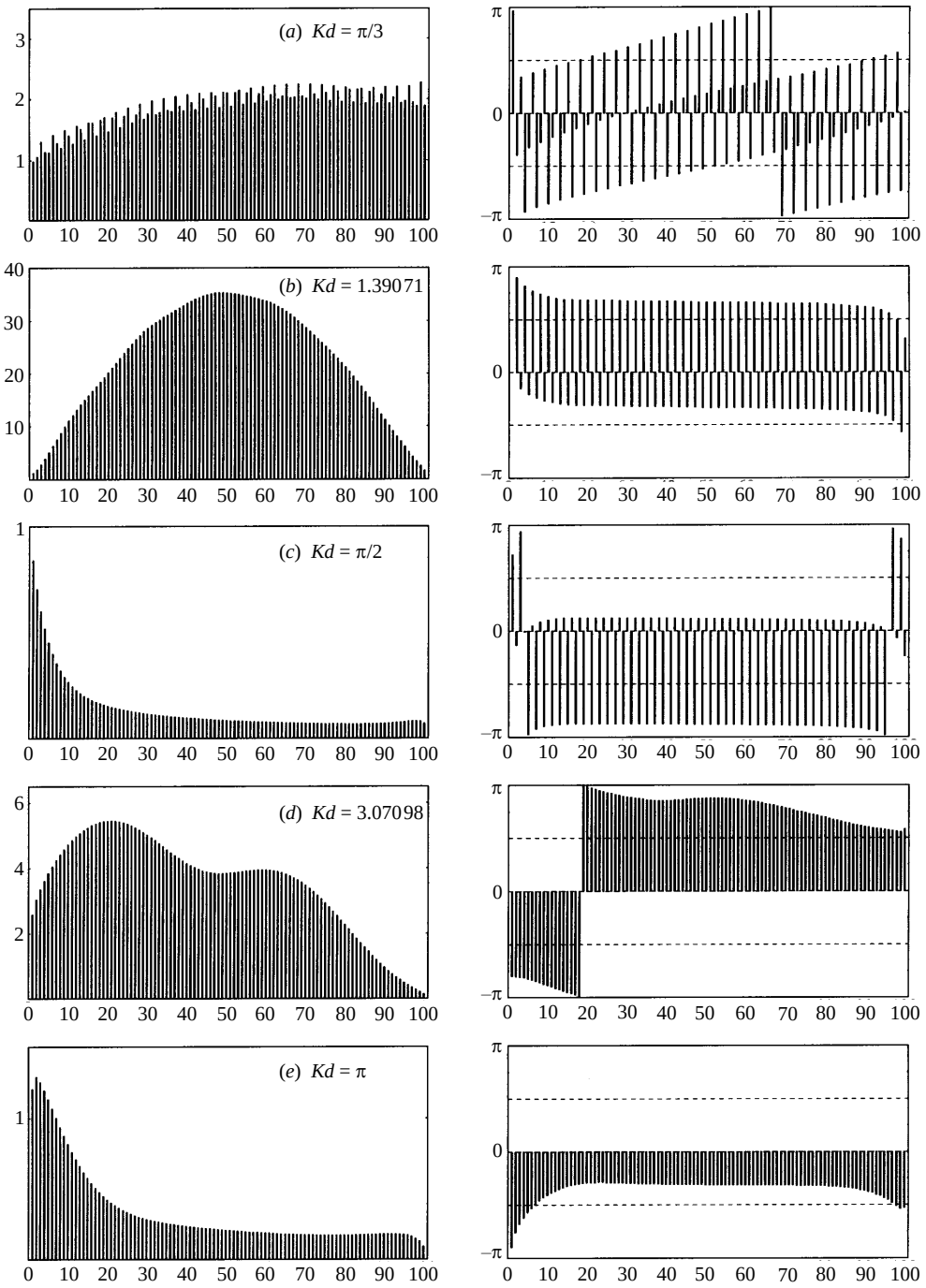

FIGURE 2. The distribution of the force magnitude (left) and phase (right) along an array of 100 circular cylinders in head seas. The diameter/spacing ratio $a/d = 1/2$. The cylinders are identified by the abscissa, with the first cylinder at the up-wave end of the array. Note that the scales of the magnitude are different in each plot.

Linton & Evans (1992), for the existence of trapped waves in the diffraction problem for a cylinder of radius a in the centre of a channel of width $2d$ when $a/d = 0.5$.

The connection between the peak loads acting on a finite array in head seas and trapped waves in a channel can be explained in the following manner. Trapped waves are known to exist in a channel, corresponding to the case of beam waves incident upon an infinite array of equally spaced cylinders. The trapped wave is associated with a homogeneous solution, of indeterminate magnitude. Since this solution is antisymmetric about the centreplane of the channel, the corresponding load on the cylinder is perpendicular to this plane.

Now consider the diffraction problem for a finite array. This can be analysed in general from the interaction theory of Linton & Evans (1990), which is re-derived below in §3. The principal result is a linear system of equations (3.7) where the unknowns are the complex amplitudes of Fourier modes at each cylinder. It is generally assumed that the same analysis applies in the limit $N \to \infty$ (see Linton & Evans 1993). However the existence of trapped waves as $N \to \infty$, for the beam-wave condition, implies that the linear system of equations which represent the interactions between the cylinders admits a homogeneous solution at the critical wavenumber where trapped waves exist, and a nearly singular solution can be expected when N is finite but large. Since the left-hand side of this linear system is independent of the wave incidence angle, the same singular behaviour can occur for head seas, or more generally for any oblique angle of incidence. From this argument we conclude that the load on each cylinder may become large at the same wavenumber where trapped waves exist in a channel, with the understanding that the channel walls correspond to the vertical planes which are normal to the axis along the array and situated midway between adjacent cylinders.

In the absence of physical walls, the velocity potential and its normal derivative must be continuous across these planes as shown in figure 4(*a*). This condition is satisfied if the local 'trapped' solution, which is antisymmetric about the plane which coincides with each cylinder axis, is nearly opposite in phase to the corresponding mode at the adjacent cylinders. It follows that the loads on adjacent cylinders will have the phase difference $\pm\pi$, as observed in case (*b*) of figure 2.

If this explanation is valid, results similar to (*b*) of figure 2 should be observed at other angles of wave incidence. This is confirmed in figure 3, where the normalized load component in line with the array is plotted at $\beta = 0$, 30°, 60°, and 90°. Even in beam waves there is a substantial in-line load, normal to the direction of wave incidence. The phase, which is omitted in figure 3, differs by approximately $\pm\pi$ between adjacent cylinders for all angles of incidence.

An exception occurs in beam waves if N is odd. This follows from symmetry, since the in-line load must be zero on the cylinder at the centre of the array. The results shown in the right column of figure 3 confirm the expectation that the cases $N = 100$ and $N = 101$ are practically identical except in beam waves.

The results shown in figures 2 and 3 were obtained using a higher-order three-dimensional spline–Galerkin panel method developed by Maniar (1995) and also described by Lee *et al.* (1996). Identical results within graphical accuracy have been computed from an independent program based on the semi-analytic theory of Linton & Evans (1990). In both methods we note that the solution is based on a linear system of equations where the influence coefficients on the left-hand side are associated with hydrodynamic interactions between different panels, or Fourier modes of the solution at each cylinder, but independent of the forcing associated with the incident wave. Thus if there is a homogeneous solution at one incident wave angle, as is known to

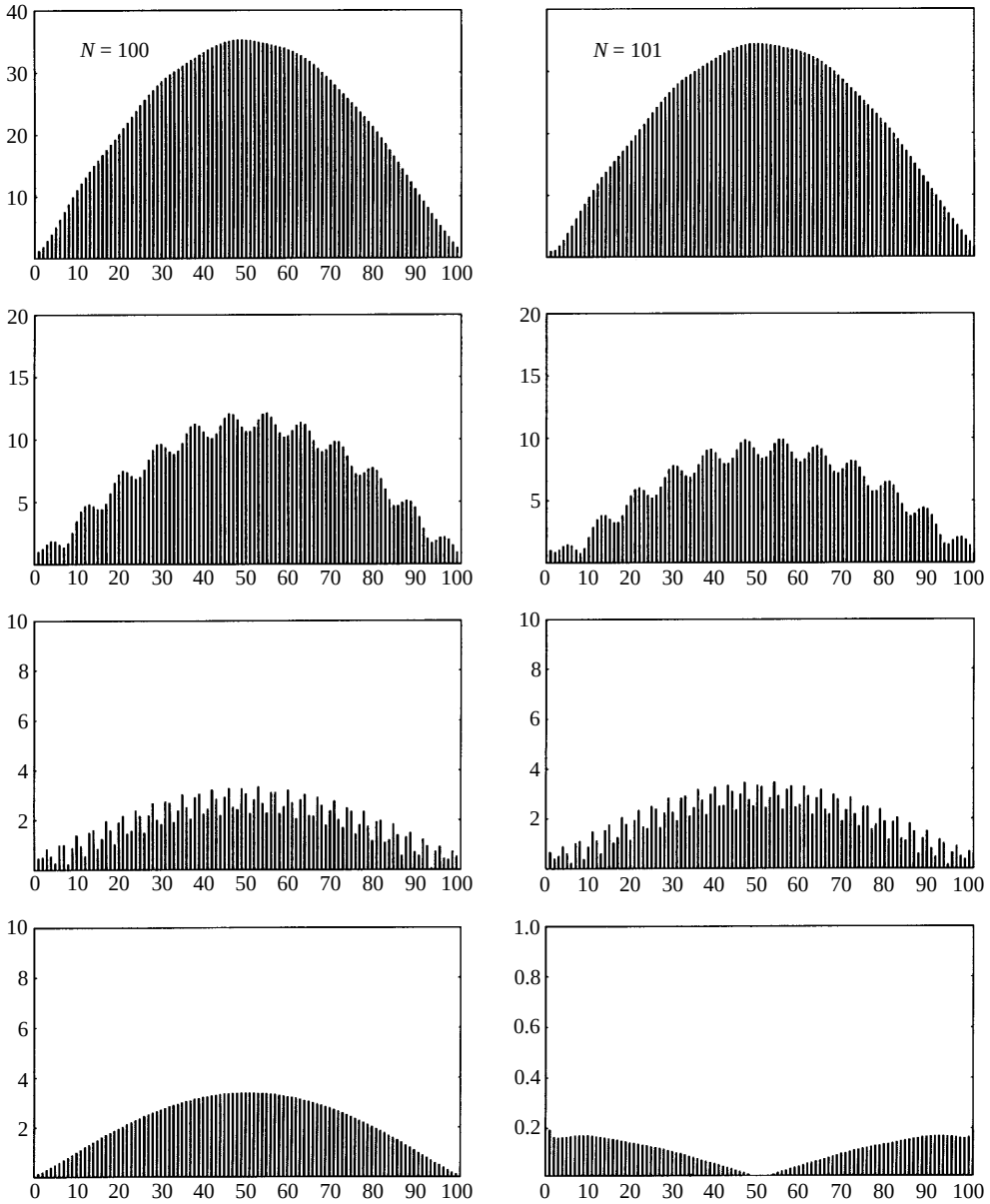

FIGURE 3. The distribution of the in-line force magnitude along an array of 100 (left) and 101 (right) circular cylinders. The in-line force is the component of the exciting force along the length of the array. From top to bottom, the four pairs of plots correspond to the incidence angles $\beta = 0, 30^\circ, 60^\circ, 90^\circ$ respectively.

exist for beam seas on an infinite array at the critical wavenumber corresponding to the first trapped mode, the same homogeneous solution will exist at the same wavenumber irrespective of the incidence angle. For an array which is large but finite, the response at this wavenumber will be nearly singular, as is observed here. This provides a heuristic explanation of the very large loads shown in figure 2(*b*) and in figure 3, and for the first peak in each of the plots shown in figure 1.

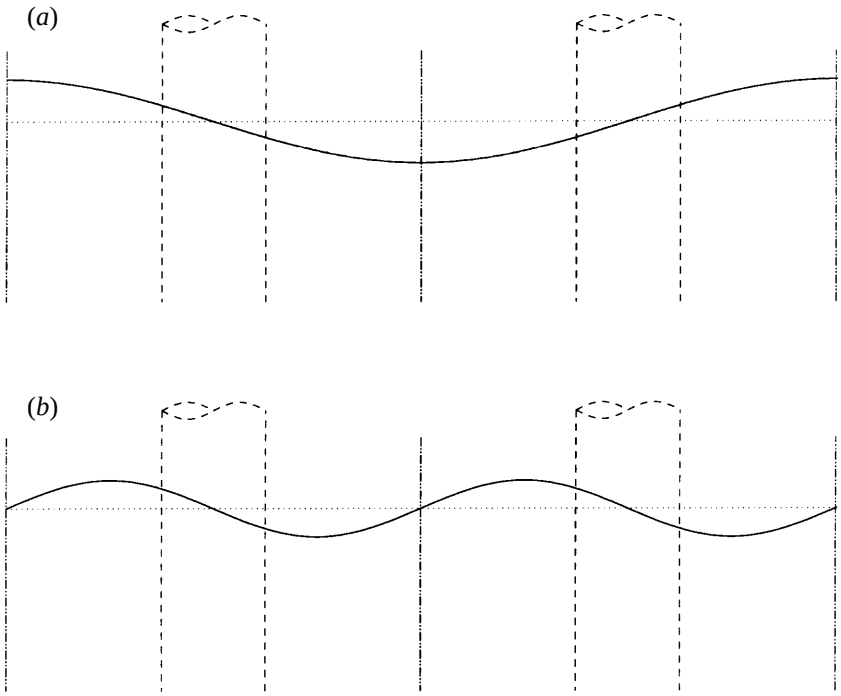

FIGURE 4. Sketches of the first Neumann (*a*) and Dirichlet (*b*) trapped modes along the array axis. The fictitious channel walls are shown as dash–dotted (— · ·—) lines, the free surface profiles as solid lines, and two adjacent cylinders as dashed (— — —) lines.

Subsequently, having observed the second peaks in figure 1, we discovered the case (*d*) in figure 2 where the maximum load on each cylinder is about five times that of a single isolated cylinder. The phase in this case is practically constant along the array, indicating a very large global force on the entire array. The analysis in §5 indicates that this case corresponds to the wavenumber of a trapped mode where homogeneous Dirichlet conditions are imposed on the channel walls. Since the potential vanishes in this case on planes midway between the cylinders, rather than the normal derivative, continuity of the solution across these planes is only possible if the adjacent solutions are in phase as shown in figure 4(*b*).

Further confirmation for the explanation in terms of antisymmetric trapped waves is apparent from figure 5, which shows contour plots of the free-surface elevation in the vicinity of the middle cylinder of the array with 101 elements, for the two wavenumbers corresponding to cases (*b*) and (*d*) in figure 2. For the Neumann case (*b*) the maximum elevation, which occurs midway between adjacent cylinders, is 35 times the elevation of the incident wave. For the Dirichlet case (*d*) the maximum elevation is 5–6 times the elevation of the incident wave, occurring on the sides of the cylinder. These very large wave motions are antisymmetric about the plane which coincides with the cylinder axis, and symmetrical or antisymmetrical, respectively, about the midplane between adjacent cylinders (satisfying homogeneous Neumann or Dirichlet conditions on the latter planes). In these respects the solution is identical to the corresponding trapped wave in a channel.

The singular interactions which are described here are not present in the analysis of an infinite array by Linton & Evans (1993). This is because the latter work assumed

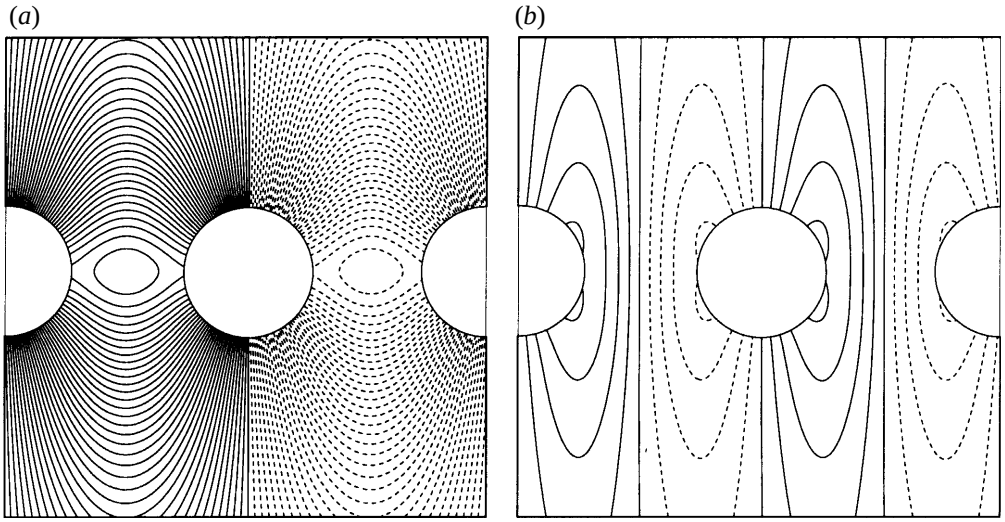

FIGURE 5. Equipotential contours at the first Neumann (*a*) and Dirichlet (*b*) trapped modes, in head waves. Only the imaginary part of the total potential is shown, for the domain near the centre of an array with 101 cylinders. Positive and negative values of the potential are indicated by solid and dashed lines respectively. The change in the potential between adjacent contours is 1.0 and $\phi = 0$ on the centreline.

periodicity of the solution with respect to both the array spacing and the wavelength of the incident waves. The latter restriction eliminated the homogeneous solution which could otherwise occur at the critical wavenumbers where trapped waves exist in a channel.

3. The interaction theory of Linton & Evans (1990)

Following Linton & Evans (1990), we consider the diffraction of plane progressive incident waves by an array of circular cylinders which extend vertically throughout the fluid domain between the free surface $z = 0$ and the bottom $z = -h$. Since the geometry is independent of the vertical coordinate and the boundary condition on each cylinder is homogeneous, the complete diffraction potential varies as a function of z in the same manner as the incident wave, and can be expressed in the form

$$\mathrm{Re}\left\{\phi_D(x, y)\, \mathrm{e}^{-\mathrm{i}\omega t} \cosh K(z + h)/\cosh Kh\right\}.$$

Here the frequency ω and wavenumber K are related by the dispersion relation $\omega = (gK \tanh Kh)^{1/2}$, where g is the gravitational acceleration. The two-dimensional function $\phi_D = \phi_I + \phi_S$ is governed by the reduced wave equation, and analogous physically to the diffraction potential for acoustic waves in two dimensions propagating past an array of circles. The component ϕ_I represents the incident wave field, and ϕ_S is the scattered field due to the array.

To simplify the notation we restrict our consideration here to an array consisting of N identical cylinders, of radius a, equally spaced along the x-axis with their axes at $x = x_j$, where $(j = 1, 2, ..., N)$ and $x_{j+1} - x_j = 2d$. Global and local polar coordinates are defined by the relations

$$x + \mathrm{i}y = r\, \mathrm{e}^{\mathrm{i}\theta}, \qquad (x - x_j) + \mathrm{i}y = r_j\, \mathrm{e}^{\mathrm{i}\theta_j}.$$

The incident-wave field can be expressed in the alternative forms

$$\begin{aligned}\phi_I &= \mathrm{e}^{\mathrm{i}K(x\cos\beta+y\sin\beta)} = \mathrm{e}^{\mathrm{i}Kr\cos(\theta-\beta)} \\ &= \sum_{n=-\infty}^{\infty} J_n(Kr)\exp\big(\mathrm{i}n(\theta-\beta+\pi/2)\big) \\ &= I_j \sum_{n=-\infty}^{\infty} J_n(Kr_j)\exp\big(\mathrm{i}n(\theta_j-\beta+\pi/2)\big)\,. \end{aligned} \tag{3.1}$$

Here J_n denotes the Bessel function of the first kind, and

$$I_j = \mathrm{e}^{\mathrm{i}Kx_j\cos\beta}$$

is the incident-wave phase at the axis of the jth cylinder.

The scattering potential associated with the jth cylinder is expressed in the corresponding form

$$\phi_S^j = \sum_{n=-\infty}^{\infty} A_n^j Z_n H_n(Kr_j)\,\mathrm{e}^{\mathrm{i}n\theta_j}, \tag{3.2}$$

where $H_n \equiv J_n + \mathrm{i}Y_n$ denotes the Hankel function of the first kind, and the factor

$$Z_n = J_n'(Ka)/H_n'(Ka) \tag{3.3}$$

is introduced for convenience later in satisfying the boundary condition of zero radial velocity on each cylinder. Note that each term in (3.2) is singular at the cylinder axis, and in the far field the radiation condition of outgoing waves is satisfied. The coefficients A_n^j are unknown at this stage.

The total scattering potential of the array is the sum of (3.2) over all elements of the array, since this is the most general solution which contains the same singularities at each cylinder while satisfying the radiation condition in the far field. After adding the incident potential (3.1), the total diffraction solution is given in the 'global' form

$$\phi_D = \phi_I + \sum_{j=1}^{N}\sum_{n=-\infty}^{\infty} A_n^j Z_n H_n(Kr_j)\,\mathrm{e}^{\mathrm{i}n\theta_j}. \tag{3.4}$$

The function (3.4) can be expressed in terms of the local coordinates of the kth cylinder using Graf's addition theorem (cf. Abramowitz & Stegun 1964, equation 9.1.79). In the domain $r_k < 2d$ it follows that

$$\begin{aligned}\phi_D = {} & I_k \sum_{n=-\infty}^{\infty} J_n(Kr_k)\exp\big(\mathrm{i}n(\theta_k-\beta+\pi/2)\big) \\ & + \sum_{j=1}^{N}{}' \sum_{n=-\infty}^{\infty}\sum_{v=-\infty}^{\infty} (\pm 1)^{n+v} A_n^j Z_n H_{n+v}(K|x_j-x_k|)J_v(Kr_k)\,\mathrm{e}^{\mathrm{i}v(\pi-\theta_k)} \\ & + \sum_{n=-\infty}^{\infty} A_n^k Z_n H_n(Kr_k)\,\mathrm{e}^{\mathrm{i}n\theta_k}. \end{aligned} \tag{3.5}$$

Here Σ' denotes summation over the array excluding the cylinder $j = k$, and the $\pm$ sign is chosen according as $k \gtrless j$ respectively.

The unknown coefficients A_n^j are determined by imposing the boundary condition of zero radial velocity on each cylinder. In the derivation of Linton & Evans (1990),

(3.5) is differentiated with respect to r_k and set equal to zero on $r_k = a$. Here we adopt a simpler approach, anticipating that the most general 'local' solution near the kth cylinder, which satisfies the homogeneous boundary condition of zero radial velocity on this cylinder, can be expressed in the form

$$\phi_D(r_k, \theta_k) = \sum_{n=-\infty}^{\infty} A_n^k \left[Z_n H_n(K r_k) - J_n(K r_k)\right] \mathrm{e}^{\mathrm{i}n\theta_k}. \tag{3.6}$$

This formula is justified on the basis that the singular contributions from the Hankel functions H_n are identical to (3.2), and the regular contributions from the Bessel functions J_n ensure that the radial derivative of each term vanishes on $r_k = a$. The latter contribution represents the local field due to the incident wave and the scattered waves from all other cylinders. The same result is derived by Evans & Linton (1990), after proceeding more directly by radial differentiation of (3.5).

On each cylinder (3.5) and (3.6) must be equal, and equating the Fourier coefficients with the same harmonic in θ_k gives the following linear system of equations for the unknown coefficients A_n^j:

$$A_m^k + \sum_{j=1}^{N}{}' \sum_{n=-\infty}^{\infty} (\pm 1)^{n-m} A_n^j Z_n H_{n-m}(K|x_j - x_k|) = -I_k \, \mathrm{i}^m \, \mathrm{e}^{-\mathrm{i}m\beta}. \tag{3.7}$$

Here $(k = 1, 2, \ldots, N)$ and $(m = 0, \pm 1, \pm 2, \ldots, \pm\infty)$.

The linear system (3.7) is identical to equation (2.11) of Linton & Evans (1990) and, after truncation to a finite number of Fourier modes $(-M \leqslant m \leqslant M)$, to their equation (2.15). In this truncated form the linear system can be solved for the unknowns A_m^k. The right-hand side of (3.7) represents the forcing due to the incident wave field, which depends on the incidence angle β. The coefficients on the left-hand side of (3.7) represent mutual interactions between different elements of the array which are independent of the incident-wave characteristics.

4. Interaction theory for large arrays

Hereafter we consider a long array ($N \gg 1$) and seek an asymptotic solution valid in the interior region far from the ends, where $1 \ll k \ll N$ in (3.7). With these assumptions the coefficients A_m^k will vary slowly with respect to the index k, except for a nearly-constant phase shift δ between adjacent cylinders. Thus we assume formally that

$$A_m^k \sim A_m^{k-1} \, \mathrm{e}^{\mathrm{i}\delta}, \tag{4.1}$$

or, to simplify the notation,

$$A_m^k \sim A_m \, \mathrm{e}^{\mathrm{i}k\delta}. \tag{4.2}$$

With this assumption (3.7) is replaced by

$$A_m + \sum_{n=-\infty}^{\infty} A_n Z_n \sum_{j \neq k} (\pm 1)^{n-m} \, \mathrm{e}^{\mathrm{i}(j-k)\delta} H_{n-m}\big(2Kd|j-k|\big) = -I_k \, \mathrm{i}^m \, \mathrm{e}^{-\mathrm{i}k\delta - \mathrm{i}m\beta}. \tag{4.3}$$

Here k is a fixed index, and the dimension of each independent linear system (4.3), for each value of k, is reduced relative to (3.7).

Let us suppose that $j = 1, 2, ..., N$ and $l = j - k$. Then (4.3) is equivalent to

$$A_m + \sum_{n=-\infty}^{\infty} A_n Z_n \left[\sum_{l=1-k}^{-1} \mathrm{e}^{\mathrm{i}l\delta} H_{n-m}\big(2|l|Kd\big) + (-1)^{n-m} \sum_{l=1}^{N-k} \mathrm{e}^{\mathrm{i}l\delta} H_{n-m}\big(2lKd\big) \right] = -I_k \, \mathrm{i}^m \, \mathrm{e}^{-\mathrm{i}k\delta - \mathrm{i}m\beta}. \tag{4.4}$$

Substituting $l = \mp j$ in the first and second sums in square brackets,

$$A_m + \sum_{n=-\infty}^{\infty} A_n Z_n \left[\sum_{j=1}^{k-1} \mathrm{e}^{-\mathrm{i}j\delta} H_{n-m}\big(2jKd\big) + (-1)^{n-m} \sum_{j=1}^{N-k} \mathrm{e}^{\mathrm{i}j\delta} H_{n-m}\big(2jKd\big) \right] = -I_k \, \mathrm{i}^m \, \mathrm{e}^{-\mathrm{i}k\delta - \mathrm{i}m\beta}. \tag{4.5}$$

With the assumptions stated above the upper limits of the inner sums in (4.5) can be set equal to ∞. The resulting Schlömilch series arise in the analysis of diffraction gratings. We shall adapt the notation of Twersky (1961) by defining the general case of this series in the form

$$\mathscr{H}_n(x, \delta) = \sum_{j=1}^{\infty} H_n(jx)\big[\mathrm{e}^{-\mathrm{i}j\delta} + (-1)^n \mathrm{e}^{\mathrm{i}j\delta}\big], \tag{4.6}$$

where x and δ are real, $x > 0$, and the series converge for all values of the arguments subject to the restriction $x \neq |\delta|$. Using (4.6), (4.5) is replaced by the simpler expression

$$A_m + \sum_{n=-\infty}^{\infty} A_n Z_n \mathscr{H}_{n-m}(2Kd, \delta) = -I_k \, \mathrm{i}^m \, \mathrm{e}^{-\mathrm{i}k\delta - \mathrm{i}m\beta}. \tag{4.7}$$

It is useful to define new unknowns which are respectively the sum and difference of $A_{\pm m}$:

$$S_m = A_m + A_{-m}, \quad D_m = A_m - A_{-m}.$$

Since $Z_n = Z_{-n}$ and $\mathscr{H}_{n-m} = (-1)^{n-m} \mathscr{H}_{m-n}$, it follows that

$$\begin{pmatrix} S_m \\ D_m \end{pmatrix} + \sum_{\substack{n=-\infty \\ n-m \text{ even}}}^{\infty} \begin{pmatrix} S_n \\ D_n \end{pmatrix} Z_n \mathscr{H}_{n-m}(2Kd, \delta) + \sum_{\substack{n=-\infty \\ n-m \text{ odd}}}^{\infty} \begin{pmatrix} D_n \\ S_n \end{pmatrix} Z_n \mathscr{H}_{n-m}(2Kd, \delta) = 2I_k \, \mathrm{e}^{-\mathrm{i}k\delta} \begin{pmatrix} -\cos m(\beta - \pi/2) \\ \mathrm{i} \sin m(\beta - \pi/2) \end{pmatrix}. \tag{4.8}$$

The in-line load on each cylinder is proportional to the coefficient D_1, and the load acting at right angles to the array is proportional to the coefficient S_1.

For an array which is very long, or infinite, one normally assumes that the phase difference δ is simply the shift in phase of the incident wave between successive cylinders:

$$\delta = 2Kd \cos\beta.$$

This is based on the assumption that the only relevant distinction between different elements is the local phase of the incident wave. Alternatively, one can argue that, since the left-hand sides of (4.7) and (4.8) are independent of k, the same must be true of the right-hand sides and thus δ is prescribed by the condition that $I_k \, \mathrm{e}^{-\mathrm{i}k\delta}$ is constant. The same restriction is applied by Linton & Evans (1993) in their analysis

of an infinitely long periodic array. On the other hand, the computational results in §§1 and 2 suggest that at certain critical wavenumbers the in-line load, and hence the coefficient D_1, are nearly resonant, implying homogeneous solutions of (4.8) where the phase of the incident wave is irrelevant. The analysis of these modes is carried out in the next section.

5. Homogeneous solutions for infinite arrays

The large loads shown in figures 1–3, and the free-surface elevations in figure 5, suggest that at certain critical wavenumbers homogeneous solutions of the linear system (4.8) exist. Two types of resonant solutions are anticipated: the Dirichlet and Neumann modes with corresponding phase differences between adjacent cylinders $\delta = 0$ or π, respectively, as discussed in §3. Thus we shall consider the existence of homogeneous solutions of (4.8) with the phase δ prescribed in advance to be either 0 or π.

For these two cases it is clear from (4.6) that the Schlömilch series are only non-zero when the order n is even. Thus the linear systems (4.8) are uncoupled, and the appropriate homogeneous form of the second system is

$$D_m + \sum_{\substack{n=-\infty \\ n-m \text{ even}}}^{\infty} D_n Z_n \mathscr{H}_{n-m}(2Kd, \delta) = 0. \tag{5.1}$$

The coefficients D_m are uncoupled for even and odd values of m, and the load proportional to D_1 can be evaluated restricting m to the set of odd integers in (5.1).

We first show that there is one homogeneous solution of (5.1) for the Dirichlet case $\delta = 0$, in the domain $Kd < \pi$, and another for the Neumann case $\delta = \pi$, in the domain $Kd < \pi/2$. The procedure we adopt for these two cases is to prove that (5.1) can be replaced by a linear system of equations with real symmetric coefficients, and then to verify numerically that the determinant of the truncated linear system vanishes at one value of Kd within the assumed domain.

Appropriate relations for the Schlömilch series are derived in the Appendix. To utilize these relations it is helpful to define $\mathscr{H}_n = \mathscr{J}_n + \mathrm{i}\mathscr{Y}_n$, as in the corresponding decomposition of the Hankel function. The results for the real component are

$$\mathscr{J}_{2n}(2Kd, 0) = -\delta_{n0} + \frac{1}{Kd} \quad (0 < Kd < \pi) \tag{5.2}$$

and

$$\mathscr{J}_{2n}(2Kd, \pi) = -\delta_{n0} \quad (0 < Kd < \pi/2), \tag{5.3}$$

where δ_{mn} is the Kroenecker delta function, i.e. $\delta_{00} = 1$ and $\delta_{n0} = 0$ for $n \neq 0$. With these results substituted in (5.1) it follows that

$$D_m(1 - Z_m) + \mathrm{i} \sum_{\substack{n=-\infty \\ n-m \text{ even}}}^{\infty} D_n Z_n \mathscr{Y}_{n-m}(2Kd, \delta) = 0. \tag{5.4}$$

There is no contribution from the sum involving the second term on the right-hand side of (5.2) since $D_{-n}Z_{-n} = -D_n Z_n$.

From the definition (3.3),

$$1 - Z_m = \mathrm{i}\, \frac{Y_m'}{J_m'}\, Z_m.$$

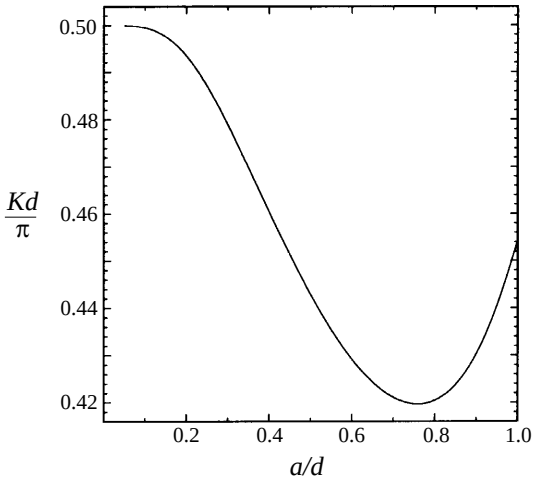

FIGURE 6. The Neumann trapped-mode wavenumber as a function of the spacing parameter (a/d). A total of four odd Fourier modes have been retained in the computations. This figure is equivalent to figure 2 of Callan *et al.* (1991).

a/d	Callan *et al.*	$N_F = 1$	$N_F = 2$	$N_F = 4$	$N_F = 8$
0.1	1.56904	1.569051	1.569051	1.569051	–
0.2	1.55023	1.550230	1.550230	1.550230	–
0.3	1.50484	1.504847	1.504842	1.504842	–
0.4	1.44655	1.446555	1.446547	1.446547	–
0.5	1.39131	1.391316	1.391314	1.391314	1.391314
0.6	1.34830	1.348305	1.348300	1.348300	1.348300
0.7	1.32288	1.322945	1.322902	1.322882	1.322882
0.8	1.32079	1.321010	1.320882	1.320789	1.320789
0.9	1.35185	1.352137	1.352110	1.351788	1.351785
1.0	1.42730	1.430229	1.427529	1.427481	1.427481

TABLE 1. Comparison of the Neumann trapped-mode wavenumber with the computations of Callan *et al.* (1991). N_F is the total number of odd Fourier modes retained in the present method.

Therefore (5.4) can be reduced to a linear system with real coefficients,

$$\frac{Y_m'}{J_m'}\left(D_m Z_m\right) + \sum_{\substack{n=-\infty \\ n-m \text{ even}}}^{\infty} \left(D_n Z_n\right) \mathscr{Y}_{n-m}(2Kd, \delta) = 0, \tag{5.5}$$

where the unknowns are the products in parentheses. In general these unknowns are complex, but the same equations apply separately to their real and imaginary parts. Thus a homogeneous solution of (4.8) will exist if and only if the determinant of the coefficient matrix in (5.5) is equal to zero.

Computations of the determinant of the truncated system are readily performed, using the formulae in the Appendix to compute the coefficients $\mathscr{Y}_{n-m}$. For the Neumann case ($\delta = \pi$) we find for all fixed values of a/d in the range ($0 < a/d < 1$) that the determinant passes through zero at one value of Kd, which varies with a/d as shown in figure 6. More precise values of this wavenumber are shown in table 1, which indicates the convergence with respect to the total number of odd Fourier modes included in the truncated version of (5.5). These values agree to a high degree

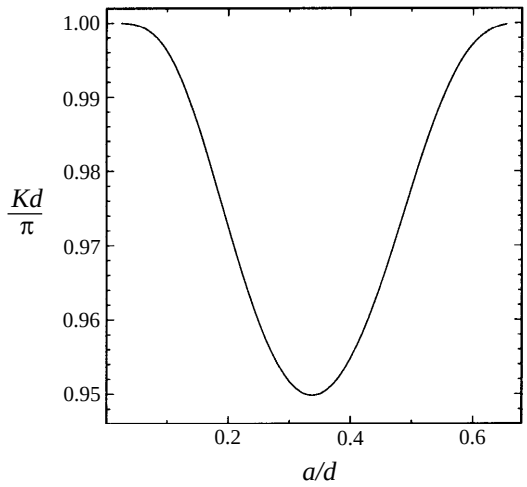

FIGURE 7. The Dirichlet trapped-mode wavenumber as a function of the spacing parameter (a/d). A total of four odd Fourier modes have been retained in the computations.

a/d	$N_F = 1$	$N_F = 2$	$N_F = 4$	$N_F = 8$
0.1	3.129606	3.129605	3.129605	3.129605
0.2	3.055237	3.055177	3.055177	3.055177
0.3	2.990391	2.989795	2.989795	2.989795
0.4	3.003034	2.999586	2.999586	2.999586
0.5	3.085486	3.071730	3.071722	3.071722
0.6	–	3.132661	3.132556	3.132556

TABLE 2. Convergence of the Dirichlet trapped wavenumber. N_F is the total number of odd Fourier modes retained in the truncated linear system.

of accuracy with those tabulated by Linton & Evans (1992). In their table 1, Linton & Evans show the results from two different computational methods, with differences beyond the second or third decimal place in the last two entries ($a/d = 0.9$ and 1.0). In these cases our results agree more closely with their second method, which is associated with the work of Callan, Linton & Evans (1991).

For the Dirichlet case ($\delta = 0$) there is likewise one zero of the determinant based on the truncated coefficient matrix in (5.5), provided a/d is in the restricted domain ($0 < a/d < 0.677$). (The latter limit is approximate.) Figure 7 and table 2 show these results. The absence of a homogeneous solution and corresponding trapped mode when $a/d > 0.677$ may be due to the proximity of the Dirichlet condition on the wall and the Neumann condition on the cylinder. When the gap between these two surfaces is small, the potential cannot change sufficiently rapidly to accomodate both boundary conditions.

The trapped-mode wavenumbers for the Neumann case are just below the cut-off $Kd = \pi/2$ for antisymmetric waves in a channel with Neumann boundary conditions on the walls. Similarly, the wavenumbers for the Dirichlet case are slightly less than the corresponding cut-off value $Kd = \pi$ for antisymmetric waves in a (non-physical) channel with Dirichlet boundary conditions. Since energy cannot radiate in an antisymmetric wave at these wavenumbers, these modes are trapped.

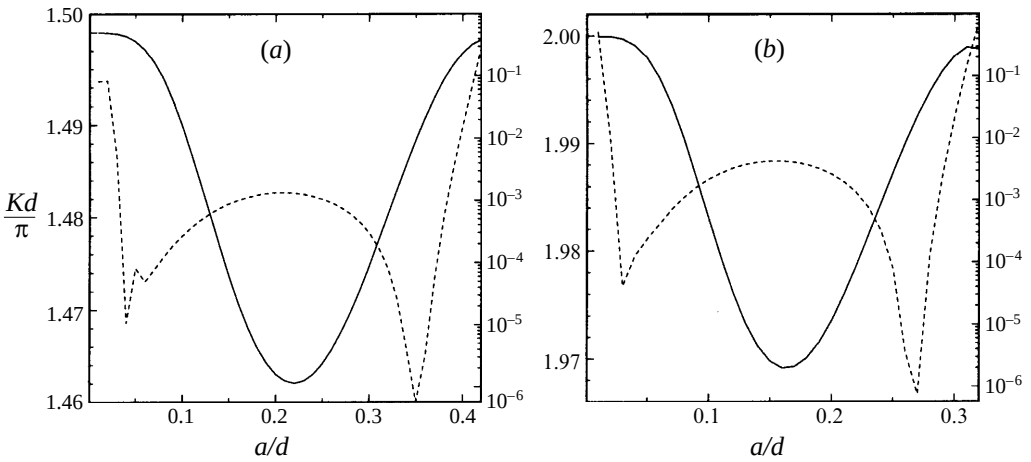

FIGURE 8. The wavenumber (solid) and determinant (dashed) as functions of the spacing parameter (a/d) at the first Neumann nearly trapped mode (a) and the first Dirichlet nearly trapped mode (b). The wavenumber and determinant correspond to the left and right ordinates respectively.

	a/d	$N=\infty$	$N=100$	$N=50$	$N=25$	$N=10$
(a)	0.1	1.569051	1.564620	1.561387	1.556078	1.535095
	0.2	1.550230	1.545296	1.537992	1.527609	1.521618
	0.3	1.504842	1.502960	1.497959	1.484591	1.455732
	0.4	1.446547	1.445607	1.442858	1.433207	1.397390
	0.5	1.391314	1.390708	1.388911	1.382053	1.346352
	0.6	1.348300	1.347841	1.346468	1.341077	1.309548
	0.7	1.322882	1.322488	1.321307	1.316623	1.287400
	0.8	1.320789	1.320405	1.319249	1.314634	1.285175
	0.9	1.351785	1.351331	1.349952	1.344432	1.310387
(b)	0.1	3.129605	3.123532	3.117117	3.109247	3.091453
	0.2	3.055177	3.053704	3.049632	3.037179	2.998946
	0.3	2.989795	2.989021	2.986778	2.978717	2.944624
	0.4	2.999586	2.998898	2.997149	2.990171	2.962101
	0.5	3.071722	3.070979	3.068774	3.063518	3.060920
	0.6	3.132556	3.130060	3.129582	3.122363	3.113582

TABLE 3. Comparison of the wavenumber of the Neumann trapped mode (a) and the Dirichlet trapped mode (b) for an infinite array ($N=\infty$) with the wavenumber at which the peak load occurs within a finite array of N cylinders.

For an array which is large but finite, pure trapping is not possible. This conclusion is based on the premise that energy radiation can occur in the three-dimensional far field, and also on the numerical results in §§1 and 2 where large but finite loads are found to occur at the peaks. Tables 3(a) and 3(b) compare the wavenumbers described above for the Neumann and Dirichlet modes of an infinite array with the wavenumbers at which the maximum peak load occurs on a finite array. Here the maximum load is defined with respect to all elements of the array. As the number of elements is increased the peak wavenumber clearly tends to the corresponding value for an infinite array. The maximum load in each case is listed in tables 4(a) and 4(b). For the Neumann mode the maximum load increases with a/d up to

	a/d	$N = 100$	$N = 50$	$N = 25$	$N = 10$
(*a*)	0.1	1.51	1.31	1.20	1.11
	0.2	5.55	2.98	1.94	1.42
	0.3	12.71	7.33	4.04	1.98
	0.4	24.08	12.11	6.80	2.89
	0.5	35.36	18.25	8.92	4.04
	0.6	46.47	22.86	12.20	5.26
	0.7	57.97	29.09	14.54	6.33
	0.8	65.44	32.79	16.35	7.00
	0.9	63.96	30.27	16.24	6.63
(*b*)	0.1	3.55	2.22	1.66	1.32
	0.2	14.66	8.14	5.14	2.34
	0.3	12.28	8.18	6.09	3.33
	0.4	6.19	5.17	4.74	2.96
	0.5	5.45	4.99	3.84	2.18
	0.6	3.07	2.10	1.83	1.65

TABLE 4. The maximum in-line force experienced by some cylinder in the array at the wavenumbers listed in (*a*) table 3(*a*) and (*b*) table 3(*b*).

approximately $a/d = 0.8$, and decreases slightly above that point. For the Dirichlet mode the maximum occurs at much smaller values of a/d. The same distinction is apparent in figure 1. For both modes the maximum load is a monotonic increasing function of the number (N) of cylinders in the array. Except for cases where the peak load is relatively small it appears that this load is proportional to N.

The possibility of higher-order trapped modes at wavenumbers $Kd > \pi$ is suggested by the numerical results shown in figure 1. This leads to the question of whether or not non-trivial homogeneous solutions of the linear system (5.1) exist for $Kd > \pi$. The analysis is more complicated in this regime since the real parts of the Schlömilch series include, in addition to (5.2) and (5.3), additional components associated with the imaginary terms in (A8) and (A9). For this reason the reduction of (5.1) to a real system is not possible. Numerical computations confirm that the modulus of the complex determinant is very small but non-zero, at wavenumbers corresponding to the higher-order peak loads of a finite array. The first higher-order wavenumbers, where the modulus of the determinant is a minimum, are shown in figures 8(*a*) and 8(*b*). Also shown are the corresponding values of the modulus of the determinant. From the latter results it is apparent that the magnitude of the higher-order peak loads is very sensitive to a/d.

6. Conclusions

A connection has been established between the existence of trapped waves in a channel and large loads acting on the elements of a long array in waves from arbitrary incidence angles. While seemingly unrelated from the physical standpoint, except in waves which are incident upon the array from abeam ($\beta = \pi/2$), these two problems share the same homogeneous solutions under more general circumstances. These homogeneous solutions exist at certain eigenvalues of the non-dimensional wavenumber Kd which depend on the ratio a/d between the cylinder diameter $2a$ and the distance $2d$ between the channel walls or the corresponding distance between adjacent cylinders in the array.

For an array which is large but finite, there are no homogeneous solutions in the strict sense, but the response in the vicinity of these wavenumbers is nearly resonant. The numerical results suggest that the peak magnitude of the load on each element increases in proportion to the total number of elements in the array. For the array with 100 cylinders the maximum load which is experienced by any cylinder in the array is 35 times the load at the same wavenumber acting on a single isolated cylinder.

The analysis here has focused on the simplest case of circular cylinders which extend vertically throughout the fluid domain from the bottom to the free surface. However the existence of trapped modes and resonant peaks can be anticipated for other types of bodies, and the essential geometrical feature is not the body shape *per se* but the periodicity of the array. Results similar to those in figure 1 are presented for an array of truncated cylinders by Lee *et al.* (1996).

The occurrence of these high loads at critical wavenumbers might have serious practical consequences for very large periodic structures, such as the proposed design for the Øresund Bridge between Denmark and Sweden. However the bandwidth of the peak loads is quite narrow, and it appears from the numerical results that the integrated effects in a continuous spectrum are not severe. This is apparent qualitatively from figure 1, and computations for larger arrays indicate that the bandwidth is inversely proportional to the magnitude of the peaks. Thus the spectral energy from these loads appears to be more-or-less independent of the number of elements in the array.

Another obvious practical consideration is that viscous damping and nonlinear effects would substantially reduce the large-amplitude motions of the free surface and associated peak loads.

The multiple peaks illustrated in figure 1 are associated not only with the Neumann mode which has been established by Callan *et al.* (1991) for a cylinder in a channel with rigid walls, but also with a corresonding Dirichlet mode corresponding to a trapped wave in a non-physical channel with zero values of the potential on the walls. However the Dirichlet mode only exists if the cylinder diameter $2a$ is less than 0.677 times the channel width or spacing between adjacent cylinder axes. Also present are several smaller peaks at higher wavenumbers. These correspond to weakly damped modes where the radiation is small but non-zero, as indicated by non-vanishing but very small values of the determinant for the corresponding linear system of equations studied in §5.

These different critical modes are closely related to the 'Parker modes' of aerodynamic resonance, generally associated with a cascade of aerofoils (or flat plates) in a wind tunnel. For such a geometry Parker (1966, 1967) showed that four different resonant modes exist with nodes (Dirichlet) or anti-nodes (Neumann) on the boundaries midway between the plates, and also on the symmetry axis normal to the flat plates at their mid-chord points. For the circular cylinder we find only the two modes which are symmetrical about the plane joining the axes. This is consistent with the conclusion of Callan *et al.* (1991), that there is no trapped mode for the circular cylinder antisymmetric about the latter plane, although such modes are shown to exist for bodies which are elongated in the direction of the channel.

As noted in the Introduction, Ohkusu (1982) has considered the reflection and transmission of waves past one or two circular cylinders situated on the centreplane in a channel. Sharp peaks are noted for the local wave elevation, particularly for the case of two cylinders. However these peaks occur in the vicinity of $Ka = 1.25$, and since $a/d = 2/5.7 = 0.351$ it follows that $Kd = 3.56$. This is substantially higher than the (Neumann) trapped mode which would occur near $Kd = 1.47$ for a single

cylinder. Another difference in Ohkusu's results is that the peaked response exists on the channel centreline, as well as on the walls, and hence his phenomenon is not associated with a strictly antisymmetric mode analogous to the trapped waves which vanish on the centreline. We have not looked for modes which are symmetric about this line since these do not affect the loads on the cylinders.

In the case of head-sea diffraction ($\beta = 0$) the approximations for a large array introduced in §4 are not valid. In particular, under the assumption that the phase of the motion at each cylinder is correlated with the incident wave ($\delta = 2Kd$), the first inner sum in (4.5) is singular when the upper limit is replaced by ∞, and it is necessary to reconsider the analysis assuming the number of elements is large but finite. From a more physical standpoint, the scattering effects from a large number of up-wave elements ($j < k$) are cumulative due to the phase correlation of their radiated waves on the kth cylinder.

The emphasis here has been on large arrays, but it is important from the standpoint of applications to note that tension-leg platforms with only two columns in line experience their maximum horizontal loads at wavelengths which are slightly longer than the spacing between the column axes. A common explanation for this peak load is based on the elementary concept of phase correlation between the incident waves and the two columns, but the slight shift to a longer wavelength coincides with the wavenumber of the first Dirichlet trapped mode. Moreover the amplification of this peak load is substantially greater than one would expect from simple arguments. Thus it appears that the trapped-wave analogy has an important application even in this relatively short array. However for a typical platform with a rectangular array of four columns the interactions between all four elements may be important, as suggested by the work of Evans & Porter (1997).

The authors acknowledge several stimulating discussions with Professor D. V. Evans and Dr R. Porter. This work was conducted under a Joint Industry Project sponsored by the Chevron Petroleum Technology Company, David Taylor Model Basin, Exxon Production Research, Mobil Oil Company, Norsk Hydro, Offshore Technology Research Center, Petrobrás, Saga Petroleum, Shell Development Company, Statoil, and Det Norske Veritas Research.

Appendix. The Schlömilch series

For the Dirichlet and Neumann cases where the relative phase δ is equal to 0 or π, the series which must be evaluated in (4.6) are

$$\mathscr{H}_\nu(2Kd, 0) = 2\sum_{j=1}^{\infty} H_\nu\big(2jKd\big) \tag{A 1}$$

and

$$\mathscr{H}_\nu(2Kd, \pi) = 2\sum_{j=1}^{\infty}(-1)^j H_\nu\big(2jKd\big), \tag{A 2}$$

respectively. Since the even and odd terms in (A 2) can be summed separately, it follows that

$$\mathscr{H}_\nu(2Kd, \pi) = -\mathscr{H}_\nu(2Kd, 0) + 2\mathscr{H}_\nu(4Kd, 0), \tag{A 3}$$

and thus it suffices to develop appropriate algorithms for the function defined by (A 1). We are concerned only with the cases where the index v is an even integer or zero.

General algorithms for evaluating these sums are derived by Twersky (1961), but it is simpler to follow the subsequent work of Miles (1983, Appendix A), starting with the definitions

$$S_v(z) = 2\sum_{j=1}^{\infty} K_v(jz) = \pi \mathrm{i}^{v+1} \sum_{j=1}^{\infty} H_v(j\,\mathrm{i}z), \tag{A 4}$$

or

$$\mathscr{H}_v(2Kd, 0) = \frac{2}{\pi}\mathrm{i}^{-v-1} S_v(-\mathrm{i}2Kd). \tag{A 5}$$

Using the formulae given by Miles, and making the substitution $Kd = \pi x$,

$$\begin{aligned}\mathscr{H}_0(2\pi x, 0) &= -(2\mathrm{i}/\pi) S_0(-2\mathrm{i}\pi x) \\ &= (1/\pi x) - 1 - (2\mathrm{i}/\pi)\left[\log \tfrac{1}{2}x + \gamma + \boldsymbol{F}_0(x)\right]\end{aligned} \tag{A 6}$$

and

$$\begin{aligned}\mathscr{H}_{2n}(2\pi x, 0) &= -(2\mathrm{i}/\pi)(-1)^n S_{2n}(-2\mathrm{i}\pi x) \\ &= (1/\pi x) + (\mathrm{i}/\pi)\Big[\frac{1}{n} + \sum_{m=1}^{n}(-1)^m \frac{2^{2m}(n+m-1)!\,B_{2m}}{(2m)!\,(n-m)!} x^{-2m} \\ &\qquad -2(-1)^n \boldsymbol{F}_{2n}(x)\Big].\end{aligned} \tag{A 7}$$

Here B_{2m} are the Bernoulli numbers and (with a convention different from Miles) $\gamma = 0.577...$ is Euler's constant. The functions $\boldsymbol{F}_n(x)$ are defined by the infinite series

$$\boldsymbol{F}_0(x) = \sum_{m=1}^{\infty}\left[(m^2 - x^2)^{-1/2} - m^{-1}\right], \tag{A 8}$$

$$\boldsymbol{F}_{2n}(x) = \sum_{m=1}^{\infty} \frac{\left[m - (m^2 - x^2)^{1/2}\right]^{2n}}{x^{2n}(m^2 - x^2)^{1/2}}. \tag{A 9}$$

For $Kd < \pi$ in the Dirichlet case, and $Kd < \pi/2$ in the Neumann case, $x < 1$ and the functions $\boldsymbol{F}_n$ are real. This accounts for the simple results (5.2) and (5.3), leading to the conclusion that the coefficients in (5.5) are real.

For $x > 1$ the appropriate branch of the square root in (A 8) and (A 9) can be determined by noting that (A 4) is analytic for $\mathrm{Re}(z) > 0$; thus, as z approaches the negative imaginary axis, the appropriate value of the square root is

$$\left[m^2 + (z/2\pi)^2\right]^{1/2} \to \left[m^2 - x^2\right]^{1/2} \quad (0 < x < m), \tag{A 10}$$

$$\left[m^2 + (z/2\pi)^2\right]^{1/2} \to -\mathrm{i}\left[x^2 - m^2\right]^{1/2} \quad (x > m). \tag{A 11}$$

With this precaution equations (A 8) and (A 9) can be used for all non-integer values of x. For $x > 1$ the terms with $m < x$ are complex, contributing to both the real and imaginary parts of (A 1).

For large m the terms in (A 8) and (A 9) are asymptotic to $\frac{1}{2}(x^2/m^3)$ and $\frac{1}{2}(x^n/m^{n+1})$,

respectively. For $\boldsymbol{F}_0$ and $\boldsymbol{F}_2$ the convergence can be accelerated by subtracting the corresponding asymptotic component from each term, and adding to this modified series the product of the Riemann zeta function $\zeta(3)$ and the factor $\frac{1}{2}x^2$ or $\frac{1}{4}x^2$, respectively. The resulting modified series, and the unmodified series for $n \geqslant 4$, converge sufficiently rapidly so that truncation is practical. (In the program developed for this purpose an absolute tolerance of 10^{-14} is used to test for convergence of the modified series for $v = 0$; the same number of terms are included in the series for $v \geqslant 2$, which converge more rapidly.)

When x tends to an integer M (A 8) and (A 9) are dominated by the singular term $m = M$. For the series (A 1) it follows that, if $Kd/\pi = x$ is close to an integer M,

$$\mathscr{H}_{2n}(2Kd, 0) \sim -2\mathrm{i}(-1)^n \left[(\pi M)^2 - (Kd)^2\right]^{-1/2}. \tag{A 12}$$

For (A 2) the last term in (A 3) is singular when $Kd/\pi = x \to M - \frac{1}{2}$, hence

$$\mathscr{H}_{2n}(2Kd, \pi) \sim -2\mathrm{i}(-1)^n \left[\pi^2(M - \tfrac{1}{2})^2 - (Kd)^2\right]^{-1/2} \tag{A 13}$$

When $Kd/\pi \to M$, the two singularities cancel in (A 3), with the result that (A 2) is finite.

REFERENCES

Abramowitz, M. & Stegun, I. A. 1964 *Handbook of Mathematical Functions with Formulas, Graphs, and Mathematical Tables*, US Government Printing Office and Dover.

Callan, M., Linton, C. M. & Evans D. V. 1991 Trapped modes in two-dimensional waveguides. *J. Fluid Mech.* **229**, 51–64.

Evans, D. V., Levitin, M. & Vassiliev, D. 1994 Existence theorems for trapped modes. *J. Fluid Mech.* **261**, 21–31.

Evans, D. V. & Porter, R. 1997 Trapped modes about multiple cylinders in a channel. *J. Fluid Mech.* **339**, 331–356.

Havelock, T. H. 1940 The pressure of water waves upon a fixed obstacle on water. *Proc. R. Soc. Lond.* A, **175**, 409–421.

Kagemoto, H. & Yue, D. K. P. 1986 Interactions among multiple three-dimensional bodies in water waves: an exact algebraic method. *J. Fluid Mech.* **166**, 189–209.

Lee, C.-H., Maniar, H. D., Newman, J. N. & Zhu, X. 1996 Computations of wave loads using a B-spline panel method. *Proc. 21st Symp. on Naval Hydrodynamics, Trondheim, Norway* (ed. O. M. Faltinsen). National Academy Press, Washington DC.

Linton, C. M. & Evans, D. V. 1990 The interaction of waves with arrays of vertical circular cylinders. *J. Fluid Mech.* **215**, 549–569.

Linton, C. M. & Evans, D. V. 1992 Integral equations for a class of problems concerning obstacles in waveguides. *J. Fluid Mech.* **245**, 349–365.

Linton, C. M. & Evans, D. V. 1993 The interaction of waves with a row of circular cylinders. *J. Fluid Mech.* **251**, 687–708.

Maniar, H. D. 1995 A three dimensional higher order panel method based on B-splines. PhD. Thesis, Massachusetts Institute of Technology.

Miles, J. 1983 Surface-wave diffraction by a periodic row of submerged ducts. *J. Fluid Mech.* **128**, 155–180.

Ohkusu, M. 1974 Hydrodynamic forces on multiple cylinders in waves. In *Proc. Intl Symp. on Dynamics of Marine Vehicles and Structures in Waves, University College, London* (ed. R. E. D. Bishop & W. G. Price), pp. 107–112. Mechanical Engineering Pub. Limited, 1 Birdcage Walk, Westminster, London.

Ohkusu, M. 1982 Reflection & transmission of waves by a row of vertical cylinders. *Bull. Res. Inst. App. Mech., University of Kyushu, Japan*, No. 57.

Parker, R. 1966 Resonance effects in wake shedding from parallel plates: some experimental observations. *J. Sound Vib.* **4**, 62–72.

PARKER, R. 1967 Resonance effects in wake shedding from parallel plates: calculation of resonant frequencies. *J. Sound Vib.* **5**, 330–343.

SIMON, M. 1982 Multiple scattering in arrays of axisymmetric wave-energy devies. Part 1. A matrix method using a plane-wave approximation. *J. Fluid Mech.* **120**, 1–25.

TWERSKY, V. 1961 Elementary function representations of Schlömlich series. *Arch. Rat. Mech. Anal.* **8**, 323–332.